

Nanoscale

Accepted Manuscript



This is an *Accepted Manuscript*, which has been through the Royal Society of Chemistry peer review process and has been accepted for publication.

Accepted Manuscripts are published online shortly after acceptance, before technical editing, formatting and proof reading. Using this free service, authors can make their results available to the community, in citable form, before we publish the edited article. We will replace this *Accepted Manuscript* with the edited and formatted *Advance Article* as soon as it is available.

You can find more information about *Accepted Manuscripts* in the [Information for Authors](#).

Please note that technical editing may introduce minor changes to the text and/or graphics, which may alter content. The journal's standard [Terms & Conditions](#) and the [Ethical guidelines](#) still apply. In no event shall the Royal Society of Chemistry be held responsible for any errors or omissions in this *Accepted Manuscript* or any consequences arising from the use of any information it contains.



Journal Name

COMMUNICATION

Nano-scale, planar and multi-tiered current pathways from carbon nanotube-copper with high conductivity, ampacity and stability

Received 00th January 20xx,
Accepted 00th January 20xx

DOI: 10.1039/x0xx00000x

www.rsc.org/

Chandramouli Subramaniam,^{*a} Atsuko Sekiguchi,^b Takeo Yamada^b, Don N. Futaba^b and Kenji Hata^{*b}

New, lithographically process-able materials with high ampacity are in demand to meet the increasing requirement of high operational current density at high temperatures existing in current pathways within electronic devices. To meet this demand, we report an approach to fabricate a high ampacity (~100 times higher than Cu) carbon nanotube-copper (CNT-Cu) composite into a variety of complex nano-scale, planar and multi-tiered current pathways. The approach involved the use of two-stage electrodeposition of copper into a pre-patterned template of porous, thin CNT sheet acting as electrode. The versatility of this approach enabled realization of completely suspended multi-tier, dielectric-less ‘air-gap’ CNT-Cu circuits that could be electrically isolated from each other and are challenging to fabricate with pure Cu or any metal. Importantly, all such complex structures, ranging from 500 nm to 20 μm in width, exhibited ~100-times higher ampacity than any known metal, with comparable electrical conductivity as Cu. In addition, CNT-Cu structures also exhibited superior temperature stability compared to the ~10-times wider Cu counterparts. We believe that the combination of our approach and the properties demonstrated here are vital achievements for future development of efficient and powerful electrical devices.

Introduction

Rapid advancements in electronics have been realized following the paradigms of Moore’s law and miniaturization.¹ The paradigm of Moore’s law has led more devices and components to operate in increasingly confined spaces.² This creates energy localizations, where devices operate in extreme conditions, such as high temperature and high current density.³ This imposes severe operating conditions on the electrical pathways to, from, and within

these energy localizations, with the demand rapidly approaching the maximum current-carrying-capacity (i.e. ampacity) limits of metals.⁴ In fact, the International Technology Roadmap for Semiconductors (ITRS) estimates that the current density in devices will exceed the ampacities of Cu and Au (~10⁶ Acm⁻²) by 2015.⁵ Therefore, an alternative electrical conductor with high ampacity in addition to performing reliably at high temperatures is in immediate demand.

Electro-migration and resultant thermal-migration are the primary mechanisms limiting the performance of metals at high current densities and high temperatures.⁶ Electromigration refers to the migration and mass-transport of atoms of conducting elements, induced by large current density and is prominent in metallic conductors such as Cu, Al and Au due to their loosely bound metallic bonds.⁶ This simultaneously increases the temperature of the conductor by Joule heating, leading to thermal-migration and consequent failure.⁷ In contrast, the strong covalent bond of carbon materials, such as carbon nanotubes⁸ (CNTs) and graphene⁹, provides a much higher ampacity (10⁸~10⁹ Acm⁻²). However, the discrete density of states results in lower conductivity when compared to metals such as Cu and Au.^{8,9} Therefore, avoiding these two failure pathways is of significant scientific and technological interest for the development of electronic devices.

A promising approach is to synergistically combine CNT and Cu while preserving the strengths (ampacity and conductivity respectively) of each material. It has demonstrated that making a CNT-Cu composite could combine the strengths of both Cu and CNTs.¹⁰ We recently demonstrated the fabrication of a CNT-Cu composite which exhibited comparable electrical and thermal conductivity as pure Cu while possessing a 100-fold higher ampacity than Cu¹⁰ and a coefficient of thermal expansion (CTE) close to Si.¹¹ While these properties of a bulk CNT-Cu composite are very promising, the key challenge for the material to be used in devices is to establish its processability and patternability in to lines and circuits, through methods that are compatible with existing semiconductor techniques while simultaneously preserving the properties of the bulk CNT-Cu composite.

Addressing this challenge, we report a strategy to achieve complex nano-dimensional patterning with CNT-Cu composite. Our approach

^a Technology Research Association for Single Wall Carbon Nanotubes (TASC), Currently at Department of Chemistry, Indian Institute of Technology Bombay, Powai, Mumbai 400076, Maharashtra, India. E-mail : csbubu@chem.iitb.ac.in

^b Nanotube Research Center, National Institute of Advanced Industrial Science and Technology (AIST), Central 5, 1-1-1 Higashi, Tsukuba 305-8565, Japan. E-mail : kenji-hata@aist.go.jp.

† Electronic Supplementary Information (ESI) available: [details of any supplementary information available should be included here]. See DOI: 10.1039/x0xx00000x

is based on the combination of the transfer of self-supporting, thin, aligned CNT sheets to a substrate; patterning them into arbitrary shapes, and then using them as a porous electrode for Cu electrodeposition. This strategy enabled the fabrication of a CNT-Cu composite with nano-scale features with various sizes and shapes. Importantly, the patterned CNT-Cu features showed similar electrical conductivity ($2.5 \times 10^5 \text{ Scm}^{-1}$) and ampacity ($5.5 \times 10^8 \text{ Acm}^{-2}$) as the bulk material reported previously ($4.5 \times 10^5 \text{ Scm}^{-1}$, $6 \times 10^8 \text{ Acm}^{-2}$, respectively).^{10,11} We would like to emphasize that the fabrication method, for this material, is compatible with conventional semiconductor processes as the CNT-sheet transfer step is carried out at room temperature as thus is completely isolated from the high-temperature CNT synthesis. Besides, the maximum temperature employed during the thermal reduction step (250°C) is much lower than what large-scale integrated circuits can bear.

Experimental and Methods

Materials

Aligned CNT sheets were synthesised using the water-assisted super-growth chemical vapor deposition (CVD) technique from patterned Fe catalysts.¹² Briefly, CNTs were synthesized from Al_2O_3 (40nm)/Fe (1.5nm) catalysts sputtered on silicon wafers with C_2H_4 (100 sccm) as carbon source and water (100 to 150 ppm) as oxygen-source. The synthesis was carried out at 750°C on a fully-automated CVD furnace. The forest consisted of aligned, single-walled carbon nanotubes (CNTs, diameter $\sim 2.8 \text{ nm}$) with high purity (99%).¹² All other chemicals were purchased from Wako and used without further purification, unless specified otherwise.

Results and discussion

The fabrication of the CNT-Cu composite pathways consists of the

following major fabrications steps, as shown in Fig. 1(a). Our approach is based on the combination of the transfer of self-supporting, thin, aligned CNT sheets to a substrate; patterning them into arbitrary shapes, and then using them as a porous electrode template for Cu electrodeposition. First, aligned SWNT sheets (1 mm width, $\sim 8 \mu\text{m}$ thickness and 1 mm long; CNT diameter $\sim 3 \text{ nm}$) were synthesized by water-assisted chemical vapor deposition (CVD) from patterned Fe catalysts.¹² Second, the CNT sheets were transferred onto Si wafer (SiO_2 thickness $\sim 100 - 500 \text{ nm}$), and densified into a closely packed, aligned CNT 'wafer' (0.5 gcm^{-3} , $\sim 1 \text{ mm}$ long).¹³ Third, the CNT wafer was lithographically patterned into desired configurations in a manner[†] analogous to Si processing.¹³ Fourth, the copper was galvanostatically deposited into the pores of the CNT film patterns to form seeds by electrodeposition using an organic electrolyte (27.7 mM $\text{Cu}(\text{CH}_3\text{COO})_2$ in CH_3CN). The similarity in solubility parameters of acetonitrile ($18 \text{ MPa}^{1/2}$) and CNTs ($18.6 \text{ MPa}^{1/2}$) allowed homogeneous deposition of Cu seeds.¹⁴ Fifth, thermal reduction of the Cu seeds was performed (250°C , H_2 flow rate of 150 sccm, 3 h) to remove the oxide. Finally, Cu filling by aqueous electrodeposition was applied to complete the filling of Cu ions. The ampacity was measured on such nanoscale, conductive CNT-Cu lines and estimated to be $5.5 \times 10^8 \text{ Acm}^{-2}$ with the highest being $5.7 \times 10^8 \text{ Acm}^{-2}$, close to hundred times higher than that measured on copper of identical dimensions (Fig. 1 (b)). The CNT interstitial spaces were completely filled with copper as shown by the fractured cross-section of a pathway (Fig. 1(e), Fig. 1(f)). In fact, the continuous nature of the CNT-Cu medium could be evidenced from the unfractured, de-laminated pathways (Fig. 1(d)). Secondary electron microscopy (SEM, Fig. 1(c) and cross-sectional line-profiles (Fig. 1(i)) by confocal laser scanning microscopy (Fig. 1(h)) recorded in the same position of the sample confirmed the height and width

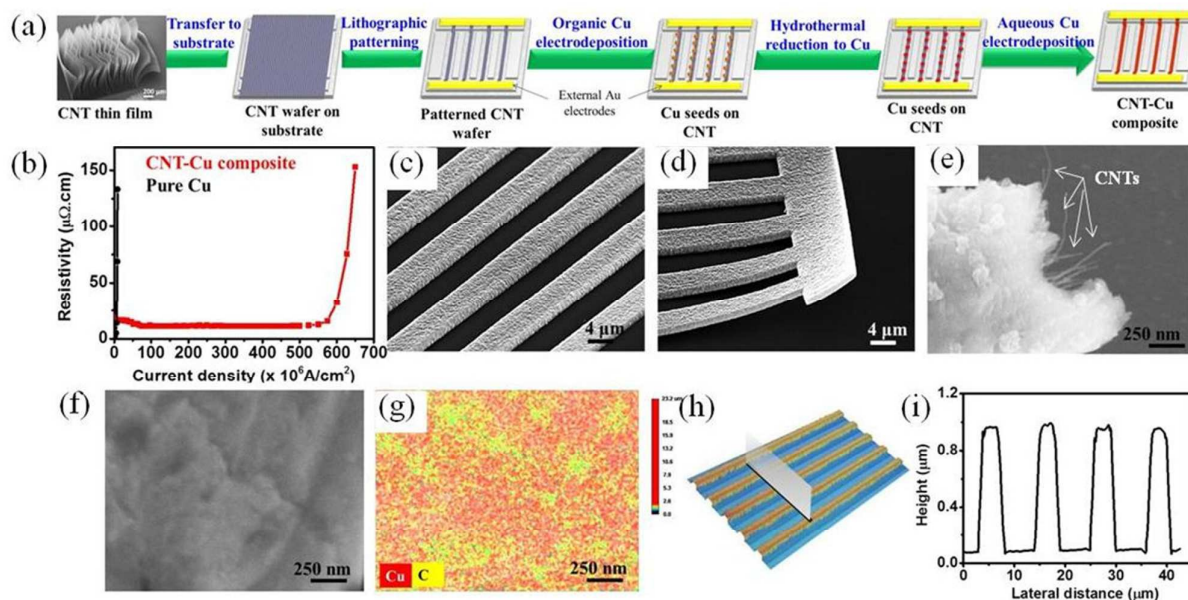


Fig. 1 (a) Schematic representation of the strategy developed for achieving sub-micron features of CNT-Cu composite. (b) Plot of resistivity versus current density for CNT-Cu composite (red trace) and Cu (black trace) confirming a ~ 100 times higher ampacity for nano-scale CNT-Cu current pathways. (c) Periodic two-dimensional current pathways with CNT-Cu composite. (d) A delaminated section of the patterned CNT-Cu composite showing structural cohesiveness and integrity. (e) and (f) represent the SEM of fractured cross-sectional surface of CNT-Cu composite with (g) presenting the EDX mapping based on Cu (red) and C (yellow). (h) Confocal laser scanning microscopy image of the CNT-Cu current pathways with the height profile shown in (i).

uniformity (1 μm thick, 4 μm width) between each conductive pathway. The microstructure of the composite exhibited good homogeneous distribution of carbon and copper as seen from energy-dispersive X-ray (EDX) analysis (Fig. 1(g)). Higher magnification imaging showed evidence of extensive interfacing between the CNTs and Cu at length-scales as low as few nanometers (~ 10 nm).

Electrical characterization revealed that the conductivity and ampacity of the macroscopic-scale composite carried over to the micro-patterned CNT-Cu pathways (1 μm thick, 4 μm wide). Room temperature 4-probe measurements showed an electrical conductivity of $2.5 \times 10^5 \text{ Scm}^{-1}$, similar to $4.5 \times 10^5 \text{ Scm}^{-1}$ for bulk CNT-Cu.^{10,11} Next, we measured the ampacity of these nano-scale structures by passing direct current through several individual line structures (0.5 μm wide, 1 μm thick) and found an average ampacity of $5.5 \times 10^8 \text{ Acm}^{-2}$ with the highest being $5.7 \times 10^8 \text{ Acm}^{-2}$ (Fig. 1(b)). This value is ~ 100 times higher than any metal (Cu, Au: $\sim 10^6 \text{ Acm}^{-2}$) and consistent with our earlier report.¹⁰ It should be noted that the coefficient of thermal expansion (CTE) of the bulk

smaller, thereby increasing the difficulty to fill the entire CNT material. In the current work, the density of thin CNT wafers was 0.5 gcm^{-3} , meaning the CNT occupied $\sim 50\%$ of the volume. This high density was required to be able to coat resist on the CNT wafer to apply standard lithography. We believe that the small physical dimensions of the pathways allowed for sufficient diffusion to deposit Cu throughout the CNT material. From this point, we could fabricate pathways with width down to 500 nm (Fig. 2(d)). Therefore, we believe further dimensional down-scaling is feasible for the composite as the Cu diffusion is facilitated by smaller template (CNT wafer) dimensions.

Our approach to fabricate high electrically conductive CNT-Cu pathways was extended to fabricate complex patterns. The CNT pattern was designed to possess an aggregate cross-sectional area approximately constant at any location between the two electrodes. In this manner, the current density passing through each segment, big or small, of the CNT pattern was kept constant, and thus Cu could be deposited uniformly. This allowed fabricating arbitrary combination of structures with filling ratios, uniformity,

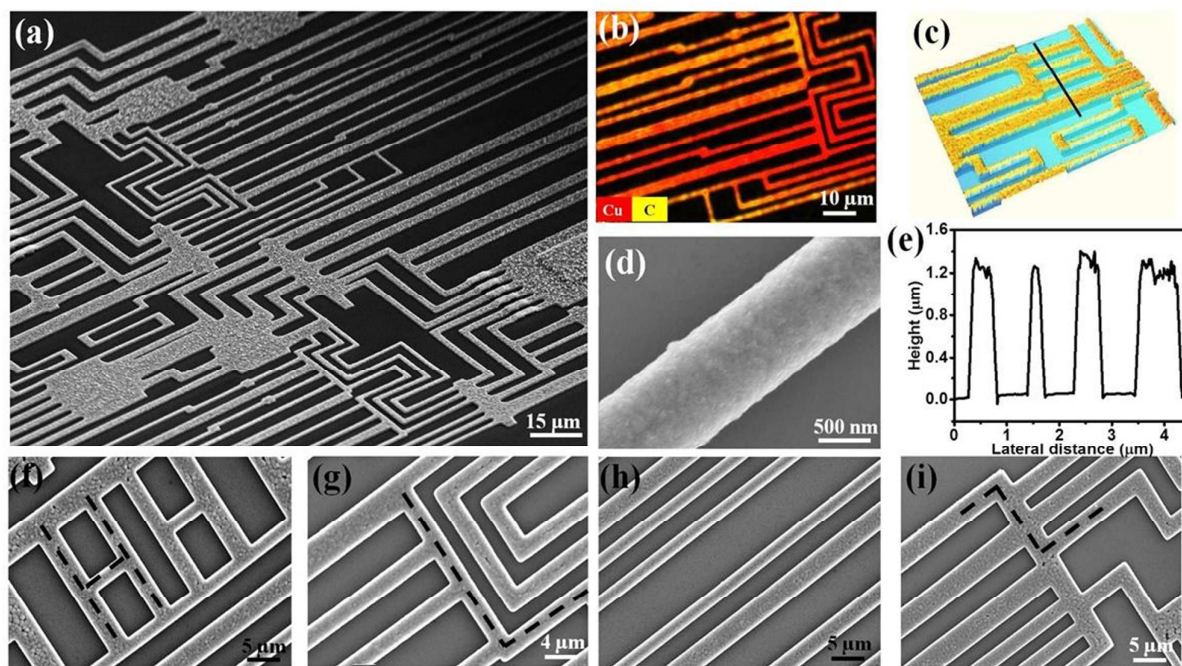


Fig. 2 (a) SEM image of complex combination of CNT-Cu current pathways consisting of arbitrary shapes and dimensions fabricated over an area of $\sim 2500 \mu\text{m}^2$ in a single batch. (b) EDX elemental mapping (based on Cu and C) of such complex combinations of current pathways. (c) Confocal laser scanning microscopic image of a portion of such patterned structures. The height profile obtained across the black line indicated is given in (e) showing the uniform height of CNT-Cu composite patterns, irrespective of their differing widths (500 nm to 1.5 μm). (d) SEM image of an isolated nano-dimensional CNT-Cu conductor showing the uniformity of the material. SEM images of several nano-scale structures with configurations such as H-shaped, L-shaped, S-shaped and their combinations thereof are presented from (f) to (i).

CNT-Cu was measured to be similar to that of silicon ($\sim 1/5^{\text{th}}$ that of copper), which is ideal for interfacing with silicon-based platforms.^{11,15} This aspect would be vital for applications such as through-silicon vias where thermal expansion mismatch between conductor and substrate is a significant problem.¹⁵

We found that the filling of the CNT interstitial spaces with Cu becomes particularly difficult when the macroscopic CNT structure is large or densely packed. Once the Cu is deposited into the interstitial spaces, the migration pathways for Cu^{2+} ions become

and homogeneity, provided the condition of constant aggregate cross-sectional area was satisfied. As demonstrated, structures with significantly different dimensions, ranging from 500 nm to 5 μm , could coexist in directions both parallel and perpendicular to the electrodes across wide areas (Fig. 2(a)). A combination of basic structures, such as bends and junctions, could be used to fabricate unique H-, L- and Z-shaped architectures with the CNT-Cu composite (Fig. 2(f) to Fig. 2(i)). Structures of varying sizes could also be fabricated, as shown by the islands distributed throughout the

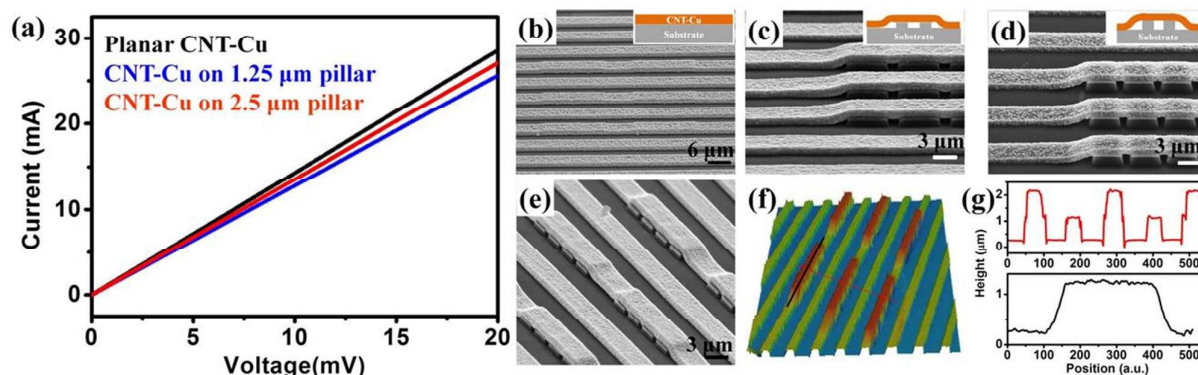


Fig. 3 (a) I-V traces of two-dimensional, planar and three-dimensional, bi-planar CNT-Cu structures fabricated over Si pillars of different heights. SEM images of multi-dimensional CNT-Cu current pathways that seamlessly traverse across different heights are given in (b) to (d). The heights of the Si pillars are 1.25 μm and 2.5 μm in (c) and (d), respectively. (e) SEM image of alternating planar and bi-planar current pathways fabricated with CNT-Cu composite. (f) Confocal laser scanning microscope image of the pattern in (e). The height profiles across the black and red lines on the image are provided in (g) and confirms the uniformity of the CNT-Cu composite pathways extending in multiple dimensions.

pattern; moreover, these islands coexisted with thin pathways, which could be fabricated from the same CNT film. The smallest feature fabricated was ~ 500 nm wide, uniform, and homogeneous (Fig. 2(d)) and could be simultaneously fabricated with the much larger structures (Fig. 2(h)). Elemental mapping by EDX indicates the presence of both Cu and C, distributed evenly along the patterns, across a wide area of the sample (Fig. 2(b)). Minor variations in the intensity distribution are attributed to the orientation of the sample during the EDX mapping. Confocal microscope images showing the cross-section of various features (ranging from widths of 500 nm to 5000 nm) indicate a similar heights, which is evidence that each CNT pattern was deposited with a similar amount of copper, and, therefore form an identical composite (Fig. 2(c), Fig. 2(e)). Our

results imply that designing suitable external electrodes would enable the fabrication of diverse variety of patterns.

The flexibility of the CNTs and the cohesiveness of the film allowed the extension of this approach to fabricate structures not possible through standard silicon based fabrication processes: suspended, three-dimensional (3-D) current pathways.¹⁶ To this end, the CNT wafer was fabricated over a Si wafer with pre-patterned silicon pillars ($1 \mu\text{m}^2$ area, 1.5 μm height) resulting in a 3-D CNT wafer that seamlessly traversed the substrate plane and elevated planes (Fig 3(c)). The CNT wafer could then be etched to form alternating suspended, bi-planar and planar pathways and subsequently converted into the composite by electrodeposition (Fig. 3(e)). In order to demonstrate the uniform electrical properties of these bi-

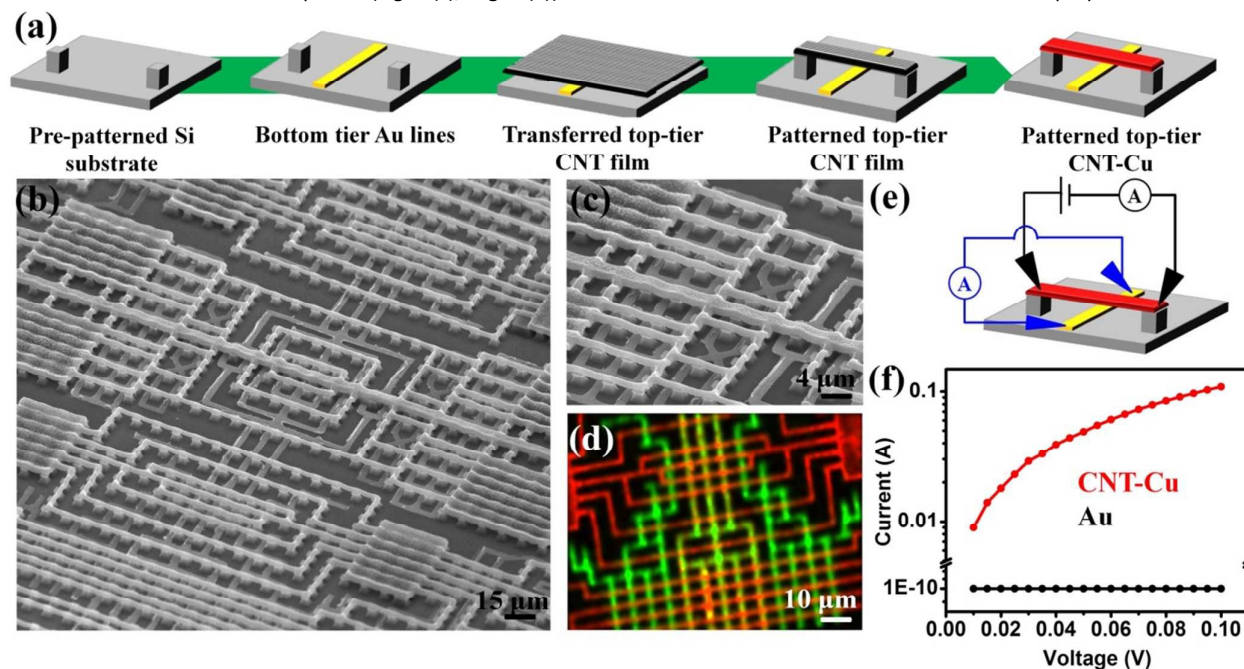


Fig. 4 (a) Schematic representation of the fabrication of multi-tier, air-gap circuits with CNT-Cu composite. (b) SEM image of the CNT-Cu composite, air-gap circuits showing the dielectric-less air-gap between the top tier of CNT-Cu composite and bottom tier Au lines. (c) The physical separation of the two tiers is seen in the SEM image. (d) EDX mapping of such air-gap separated circuits, based on Cu (red) and Au (green), reveals the absence of physical overlap between the two tiers. This is further confirmed from electrical measurements the schematic and the data of which are presented in (e) and (f), respectively.

planar lines, I-V traces across CNT-Cu structures made with Si pillars of three different heights (0 μm , 1.25 μm , and 2.5 μm) were measured and found to be identical (Fig. 3(a)). As seen from the SEM (Fig. 3(b) to Fig. 3(e)) and confocal microscope imaging (Fig. 3(f)), the height profile across these alternating patterns (Fig. 3(g), red trace) also alternates between ~ 1 and 2 μm , indicating a uniformly thick composite (~ 1 μm) for both planar and bi-planar current pathways. Furthermore, line profiles taken along a single bi-planar structure showed a seamless height transition from 0.3 μm to 1.25 μm (Fig. 3(g), black trace). As the height of the pillar was 1 μm , this further demonstrates that we were able to make a uniform material in a bi-planar configuration. These aspects demonstrated the feasibility of our approach to fabricate bi-planar CNT-Cu structures as reliable current pathways.

The potential to fabricate 3-D CNT-Cu architectures could be further extended to make multi-tiered pathways using the strategy outlined (Fig. 4(a)). An entire CNT film was suspended on silicon pillars (1.5 μm height) to form the top tier over a series of prefabricated Au pathways representing the bottom tier. The suspended CNT sheet in the top tier was etched into patterns and subsequently converted into CNT-Cu by electrodeposition. Such 3-D CNT-Cu structures could be fabricated into versatile shapes and sizes (Fig. 4(b)) despite being completely suspended with the widths of the lines varying from 1.5 μm to 5 μm (thickness ~ 1 μm). A variety of complex, fully suspended current pathways were then fabricated to include branching patterns comprising of both orientations (parallel and perpendicular) of aligned CNTs (Fig. 4(c)). The distance between the bottom Au tier and top CNT-Cu tier was estimated to be ~ 1.3 μm from the SEM images (Fig. 4(c)) which corresponded well with the height of the pillars. Further, electrical isolation between the two tiers was confirmed using the schematic in Fig. 4(e). A potential difference was applied across the top tier, consisting of CNT-Cu and the current was measured across the bottom tier. Negligible leakage current ($\sim 10^{-10}$ A, close to the resolution of the measurement system) was measured, demonstrating the electrical isolation between the upper and lower tiers (Fig. 4(f)). This was also confirmed through EDX elemental mapping that showed clear elemental separation of the bottom Au tier and the CNT-Cu pathways in the top-tier. Since, deposition of Cu on CNT proceeded through the creation of electric field, any physical contact of CNT (top-tier) with Au (bottom tier) would have resulted in Cu being deposited on Au lines as well. Therefore, the observation of distinct EDAX signatures from both Au and Cu, without any mixing, confirms the CNT-Cu is physically separated from Au tier. That is, the absence of the Cu signals on the Au lines is evidence of specific electrodeposition on the CNT lines, confirming electrical isolation between tiers (Fig. 4(d)). Our multi-tier pathways can be considered as "air-gap" circuits, with vacuum as dielectric medium between the metallization lines providing the ideal dielectric separation between them.¹⁷ Such multi-tier architectures can address to the parasitic capacitance occurring in closely-spaced metallization lines.¹⁷

In order to investigate the stability of our CNT-Cu pathways, we implemented lifetime evaluation at high current densities (10^7 - 10^8 Acm^{-2}) and temperature (250 $^\circ\text{C}$) that Cu cannot withstand (Fig. 5(a)). The mean time to failure was defined as the point of 20% decrease in conductivity and determined for two line-widths of CNT-Cu composite (500 nm and 5000 nm).¹⁸ Both the CNT-Cu

composite and Cu showed a similar behaviour, where at the initial stages the conductivity was stable, while beyond a particular time it dropped exponentially and failed. In all cases, the CNT-Cu composite showed a significantly longer lifetime, highlighting its superiority over Cu. The lifetime was estimated and plotted as a function of current density (Fig. 5(b)). Both the CNT-Cu composite and Cu showed a monotonic decrease in their lifetimes as current

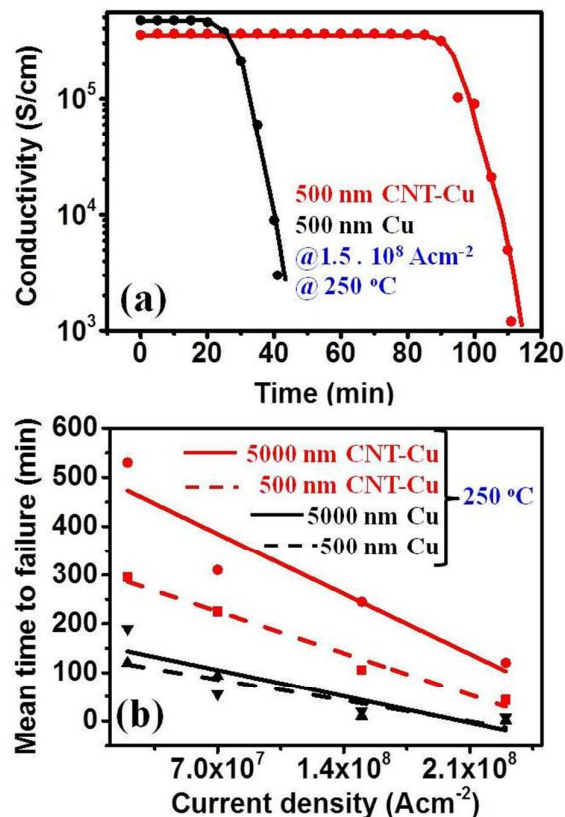


Fig. 5 (a) Time-evolution of electrical conductivity of CNT-Cu composite (red) and Cu (black) under stress conditions of 1.5×10^8 Acm^{-2} and 250 $^\circ\text{C}$. (b) Plot of mean-time-to-failure for CNT-Cu composite and Cu structures of two different dimensions (500 nm and 5000 nm width) showing a significantly superior lifetime and stability of CNT-Cu composite.

density increased, with the CNT-Cu structures always possessing a significantly longer lifetime. In particular, the CNT-Cu structures with 500 nm width exhibited longer lifetime than a 10-fold wider pure copper line (5000 nm) (Fig. 5(b)). This result implies that a 10-fold decrease in line-width is possible by replacing Cu with CNT-Cu. Although the mechanism of the high performance of the CNT-Cu lines is not yet completely well understood, theory predicts that carbon-doping into Cu would increase the activation energy of diffusion of Cu.^{10,19} The two primary mechanisms acting to achieve this are dopant-dragging¹⁹ (migration of Cu with C, resulting in increase in activation energy) and dopant-blocking¹⁹ (occupancy of Cu interstitial sites by carbon, resulting in physical obstruction of the migration pathways). We expect the CNTs to act similar to the dopant carbons; however CNTs themselves possess a very high tolerance to electromigration. Therefore, the dopant dragging mechanism is expected to be less dominant here. Thus, we expect that CNTs are blocking and suppressing Cu diffusion to yield a higher ampacity and more stable conducting composite.

Conclusions

In conclusion, we demonstrated an approach to fabricate nanoscale patterning of a CNT-Cu composite possessing the electrical conductivity on par with Cu and ampacity ~100 times higher than Cu. Through the use of an aligned CNT sheet as a porous electrode, Cu could be uniformly electrodeposited throughout the patterned sheet to create homogeneous micropatterned CNT-Cu composite. Complex bi-planar and multi-tiered, electrically isolated air gap structures could be fabricated, which are otherwise impossible by the conventional vapor deposition of Cu, thereby illustrating the strength of this approach. Importantly, the electrical conductivity and ampacity carried over from the macroscopic dimensions to the sub-micron structures. These results taken together, we believe that sustaining the properties at nanoscale dimensions as demonstrated here provides a feasible approach for utilization of CNT-Cu electrical current pathways in electronic devices.

Notes and references

‡ Patterning of CNT film

Vertically aligned CNT sheet (measuring 700 μm x 700 μm with an as-grown thickness of 8 μm) was carefully transferred to the desired substrate in the desired orientation using a liquid-induced densification approach.¹³ The CNT sheets were then transferred from the growth substrate to the target substrate. Although such CNT sheets were sparse ($\sim 0.04 \text{ g cm}^{-3}$), the long and entangled CNTs provided them with sufficient mechanical cohesiveness to allow their handling as a continuous unit for removal and transfer without damage. Thus, such CNT sheets were transferred onto Si wafer (SiO_2 thickness $\sim 100 - 500 \text{ nm}$), and densified into a closely packed, aligned CNT 'wafer' (0.5 g cm^{-3} , $\sim 1 \text{ mm}$ long) using a liquid-induced densification approach as previously described.¹³ Thickness of the CNT films after attachment to the substrate was measured to be around 700 nm. Then, the CNT wafer was patterned into desired configurations.

Positive tone PMMA-495 (Microchem Corp.) was spin coated at 4700 rpm for 60 s on the substrate followed by curing at 180 $^\circ\text{C}$ for 60 s. A double mask recipe was adapted using a negative tone FOX 16 (flowable oxide, Dow Corning) on top of the cured PMMA-495. The FOX 16 was spin coated at 4500 rpm for 60 s followed by baking at 120 $^\circ\text{C}$ for 8 minutes. Electron-beam lithography was used to expose the required areas of CNT. The substrate was developed using tetramethylammonium hydroxide (TMAH), rinsed with water and dried under a dry N_2 flow. Reactive ion etching (RIE) using a mixture of $\text{O}_2/\text{Ar}/\text{CHF}_3$ was carried out to remove the unwanted CNT areas. After the CNT patterning, the negative resist and positive resist were removed using buffered hydrogen fluoride (BHF) and 1:1 mixture of methylisobutyl ketone/isopropyl alcohol (MIBK/IPA), respectively. Finally, the substrate was rinsed in IPA and dried under N_2 stream before Cu electrodeposition.

Microfabrication of CNT-Cu composite

Metal electrodes (3 nm Ti and 100 nm Au) were fabricated by sputtering on the Si or Si_3N_4 substrates after defining the required shapes through electron beam lithography. The CNT sheets were transferred from the growth substrate to the target substrate using the liquid-induced densification approach¹³ and oriented in the desired alignment.

Copper was deposited into the pores of the CNT film patterns to form seeds by electrodeposition. Despite being densified, these patterned CNT wafer were sufficiently porous ($\sim 50\%$) to allow deposition of Cu onto all CNT surfaces, both on the periphery and in the pore volume of the wafers, to make a CNT-Cu composite that was homogeneous enough to act as single cohesive unit. Thermal reduction of the Cu seeds was performed (250 $^\circ\text{C}$, H_2 flow rate of 150 sccm, 3 h) to remove the oxide and other organic contaminations. Finally, Cu filling by aqueous electrodeposition was applied to complete the filling of Cu ions into the porous CNT template with high (55 vol%) and homogeneous filling of Cu.

- 1 U.S. Congress, Office of Technology Assessment, Miniaturization Technologies, OTA-TCT-514 (Washington, DC; U.S. Government Printing Office, November, 1991).
- 2 G.E. Moore, *Proceedings of IEEE*, 1998, **86**, 82.
- 3 J. Lienig presented at SLIP'05 International workshop on system level interconnect prediction, San Francisco, California, U.S.A. (April, 2005).
- 4 J. R. Black, *IEEE Trans. on Electron Devices*, 1969, **16**, 338.
- 5 ITRS International Technology Working Groups. International Technology Roadmap for Semiconductors, <http://www.itrs.net>, accessed May, 2015.
- 6 (a) P.S. Ho, T. Kwok, *Rep. Prog. Phys.* 1989, **52**, 301; (b) P.C. Li, T. K. Young, *IEEE Spectrum*, 1996, **33**, 75; (c) L. Pauling, *The Nature of Chemical Bond*, Cornell University Press, U.S.A, 1960.
- 7 S. Krishnan, S. V. Garimella, G. M. Chrysler, R. V. Mahajan, *IEEE Trans. Adv. Pack.* 2007, **30**, 462.
- 8 (a) Z. Yao, C. L. Kane, C. Dekker, *Phys. Rev. Lett.* 2000, **84**, 2941; (b) B.Q. Wei, R. Vajtai, P.M. Ajayan, *Appl. Phys. Lett.* 2001, **79**, 1172; P.G. Collins, M. Hersam, M. Arnold, R. Martel, P. h. Avouris, *Phys. Rev. Lett.* 2001, **86**, 3128; (c) X. Wang, N. Behabtu, C. C. Young, D. E. Tsentelovich, M. Pasquali, J. Kono, *Adv. Func. Mat.* 2014, **24**, 3241; (d) D. Janas, A. P. Herman, S. Boncel, K.K. K. Koziol, *Carbon*, 2014, **73**, 225.
- 9 (a) R. Murali, Y. Yang, K. Brenner, T. Beck, J. D. Meindl, *Appl. Phys. Lett.* 2009, **94**, 243114; (b) K. J. Lee, A. P. Chandrakasan, K. Jing, *IEEE Electr Device L.* 2011, **32**, 557; (c) A. D. Liao, J.Z. Wu, X. Wang, K. Tahy, D. Jena, H. Dai, E. Pop, *Phys. Rev. Lett.* 2011, **106**, 256801.
- 10 C. Subramaniam, T. Yamada, K. Kobashi, A. Sekiguchi, D. N. Futaba, M. Yumura, K. Hata, *Nature Commun.* 2013, **4**, 2202.
- 11 C. Subramaniam, Y. Yasuda, S. Takeya, S. Ata, A. Nishizawa, D. Futaba, T. Yamada, K. Hata, *Nanoscale*, 2014, **6**, 2669.
- 12 K. Hata, D. N. Futaba, K. Mizuno, T. Namai, M. Yumura, S. Iijima, *Science*, 2004, **306**, 1362.
- 13 (a) Y. Hayamizu, T. Yamada, K. Mizuno, R. C. Davis, D. N. Futaba, M. Yumura, K. Hata, *Nat. Nanotech.* 2008, **3**, 289; (b) T. Yamada, Y. Hayamizu, Y. Yamamoto, Y. Yomogida, A. I. Najafabadi, D. N. Futaba, K. Hata, *Nat. Nanotech.* 2011, **6**, 296; (c) T. Yamada, N. Makimoto, A. Sekiguchi, Y. Yamamoto, K. Kobashi, Y. Hayamizu, Y. Yomogida, H. Tanaka, H. Shima, H. Akinaga, D. Futaba, K. Hata, *Nano Lett.* 2012, **12**, 4540; (d) T. Yamada, Y. Yamamoto, Y. Hayamizu, A. Sekiguchi, H. Tanaka, K. Kobashi, D. N. Futaba, K. Hata, *ACS Nano*, 2013, **7**, 3177.
- 14 S. D. Bergin, Z. Sun, D. Rickard, P.V. Streich, J. P. Hamilton, J. N. Coleman *ACS Nano*, 2009, **3**, 2340.
- 15 A. Vassighi, M. Sachdev, *IEEE Trans. Device Mater. Reliab.* 2006, **6**, 300.
- 16 S. Savastouk *Solid State Technol.* 2000, **43**, 84.
- 17 L. G. Gosset, A. Farcy, J. de Pontcharra, Ph. Lyan, R. Daamen, G.J. A. M. Verheijden, V. Arnal, F. Gaillard, D. Bouchu, P. H. L.

- Bancken, T. Vandeweyer, J. Michelon, V. N. Hoang, R. J. O. M. Hoofman, J. Torres, *Microelectron Eng.* 2005, **82**, 321.
- 18 (a) J. R. Black, *IEEE Trans. Electron Dev.* 1969, **16**, 338 ; (b) J.R. Lloyd, *J. Appl. Phys.* 1991, **69**, 7601.
- 19 (a) C. L. Liu, *Appl. Phys. Lett.* 2002, **80**, 763; (b) C.L. Liu, X. Y. Liu, L.J. Borucki *Appl. Phys. Lett.* 1999, **74**, 34; (c) C. L. Liu, *Phys. Stat. Sol.* 2001, **1**, 47. (d) P. Wilhite, A. A. Vyas, J. Tan, J. Tan, T. Yamada, P. Wang, J. Park, C. Y. Yang *Semicond. Sci. Technol.* 2014, **29**, 054006. (e) M. G-Asl, P.D. Bristowe, K. Koziol *Phys. Chem. Chem. Phys.* 2015, **17**, 18273.